European Journal of Radiology 121 (2019) 108740

Contents lists available at ScienceDirect

European Journal of Radiology

journal homepage: www.elsevier.com/locate/ejrad

Research article

Association between true non-contrast and virtual non-contrast vertebral bone CT attenuation values determined using dual-layer spectral detector CT

Yuqin Ding[a,b], Andreas Richter[b], Wolfram Stiller[b,c], Hans-Ulrich Kauczor[b,c], Tim Frederik Weber[b,*]

[a] Department of Radiology, Zhongshan Hospital, Fudan University, Shanghai Institute of Medical Imaging, Shanghai, 200032, People's Republic of China
[b] Department of Diagnostic and Interventional Radiology, Heidelberg University Hospital, INF 110, 69120, Heidelberg, Germany
[c] Translational Lung Research Center Heidelberg, Member of the German Center for Lung Research, Heidelberg University Hospital, INF 156, 69120, Heidelberg, Germany

ARTICLE INFO

Keywords:
Computed tomography
Dual-energy CT
Virtual non-contrast images
Bone mineral density
Osteoporosis

ABSTRACT

Purpose: To investigate the association of vertebral CT attenuation between virtual non-contrast (VNC) and true non-contrast (TNC) images and to evaluate if VNC vertebral CT attenuation could be used for phantom-less osteoporosis detection in dual-layer spectral-detector CT (SDCT).

Methods: 200 patients with non-contrast and portal-venous phase SDCT were retrospectively assigned to a test and a validation group of 100 patients each. CT attenuation of L1 vertebrae were measured on VNC and TNC. The test group was used to determine the difference between VNC and TNC CT attenuation and to calculate a statistical model for TNC CT attenuation prediction. The validation group was used to assess the capability of the model to predict TNC from VNC CT attenuation and its accuracy to identify osteoporosis. Osteoporosis was defined as a TNC CT attenuation of ≤110HU.

Results: In both groups, CT attenuation was lower in VNC than in TNC ($P < 0.001$). VNC and TNC CT attenuation was correlated strongly ($r = 0.958$). Using the regression equation established in the test group ($TNC = 23.677 + 1.540 \times VNC$), the predicted TNC CT attenuation did not differ from the real TNC CT attenuation in the validation group ($P = 0.359$). A VNC CT attenuation cut-off of 52HU yielded an AUC of 0.978 for osteoporosis detection.

Conclusions: L1 CT attenuation is systematically underestimated in VNC compared with TNC images. However, TNC L1 CT attenuation can be predicted reliably from VNC. VNC may perform well in phantom-less osteoporosis detection.

1. Introduction

Osteoporosis as the abnormal loss of bone mineral density (BMD) is a worldwide health issue associated with risk of fractures, contributes substantially to morbidity and mortality, and carries social and economic burden [1]. It remains substantially underdiagnosed and undertreated with participation rates for dual-energy x-ray absorptiometry (DXA) of only 30 % and 4 % in eligible women and men over 65 years, respectively [2,3]. According to the World Health Organization, DXA is the standard method for BMD estimation targeting at the lumbar spine and the femoral neck [4]. Quantitative computed tomography (CT) is an alternative that uses a CT acquisition including a calibration phantom with which CT numbers in HU can be converted to BMD values. Previous studies on opportunistic osteoporosis detection using CT performed for other indications have shown that osteoporosis may be identified in conventional CT images by measuring the vertebral trabecular bone CT attenuation value without including a calibration phantom [5–9]. In a previous study with the largest patients population (n = 1867), a threshold of 110 HU for the trabecular bone of the first lumbar (L1) vertebra was more than 90 % specific for distinguishing between presence and absence of osteoporosis [7]. However, it has been shown that conventional CT-based BMD measurements can be affected by acquisition parameters such as different tube voltages and the use of intravenous contrast material [10–12]. As the administration of iodinated contrast material increases the CT attenuation value in a given vertebra and the timing of the post-contrast phase influences the

Abbreviations: TNC, true non-contrast; VNC, virtual non-contrast; SDCT, spectral detector CT; PVP, portal venous phase; BMD, bone mineral density; DXA, dual-energy x-ray absorptiometry; SBI, spectral based images

* Corresponding author.
E-mail address: tim.weber@med.uni-heidelberg.de (T.F. Weber).

https://doi.org/10.1016/j.ejrad.2019.108740
Received 4 March 2019; Received in revised form 23 August 2019; Accepted 4 November 2019
0720-048X/

CT attenuation value increase, CT attenuation value measurements are preferably performed using true non-contrast (TNC) images. The availability of TNC images, however, depends on the imaging protocol and is limited to a narrow spectrum of clinical indications.

Recently, a novel dual-layer detector CT scanner was introduced that uses two different detector layers each absorbing different parts of the polychromatic X-ray spectrum for spectral imaging and material decomposition (iQon Spectral CT, Philips Healthcare, Best, The Netherlands) [13,14]. While other dual-energy CT techniques such as dual-source CT require the pre-selection of specific dual-energy CT protocols prior to image acquisition, the dual-layer spectral detector CT (SDCT) enables retrospective spectral analyses on all acquisition protocols when images are acquired at 120 or 140 kVp and spectral raw data (spectral base images, SBI) are archived. Material decomposition using spectral data sets allows for reconstruction of virtual non-contrast (VNC) images that have been shown to be comparable to true non-contrast (TNC) images in regards of CT attenuation value of solid organs [15].

To the best of our knowledge, the comparability of CT attenuation value measurements of osseous structures between VNC and TNC images has not been assessed so far. The aim of this study is to investigate the association of vertebral bone CT attenuation values between VNC and TNC images and to evaluate if VNC vertebral bone CT attenuation values could be used for phantom-less opportunistic osteoporosis detection in SDCT scans performed for other indications.

2. Materials and methods

2.1. Study design

This is a retrospective single-center exploratory study that was approved by the institutional review board with a waiver of informed consent. Primary objective was to determine the difference in the CT attenuation value of the first lumbar vertebra between VNC images generated from portal venous phase post-contrast images (VNC L1 CT attenuation value) and TNC images (TNC L1 CT attenuation value). Secondary objectives were: (1) to assess the difference in the CT attenuation value of the abdominal aorta between VNC images (VNC aortic CT attenuation value) and TNC images (TNC aortic CT attenuation value) in order to evaluate systematic discrepancies of spectral material decomposition between osseous and non-osseous structures; (2) to establish a statistical model to predict TNC L1 CT attenuation values using VNC L1 CT attenuation values; (3) to assess the accuracy of this model for identifying osteoporosis.

For this purpose, 200 consecutive patients with SDCT examinations of the abdomen in the time period between December 2017 and April 2018 were allocated to a test group and a validation group of 100 individuals each. The test group was used to determine the difference between VNC and TNC CT attenuation values and to calculate a statistical model for TNC L1 CT attenuation value prediction. The validation group was used to verify the capability of the model to predict TNC from VNC L1 CT attenuation values and to assess the accuracy of this model to identify osteoporosis. According to Pickhardt et al. [7], the CT attenuation value threshold for osteoporosis detection was defined as a L1 CT attenuation value of 110 HU or less determined on TNC images. Inclusion criteria were: (1) availability of a SDCT examination including a true non-contrast acquisition of the abdomen and a portal venous phase (PVP) post-contrast acquisition of the abdomen and pelvis; (2) availability of SBI to generate virtual non-contrast images from PVP post-contrast acquisitions; (3) patient age at least 50 years. Exclusion criteria were: (1) structural defects of the first lumbar vertebra such as fracture or focal lesions; (2) severe image artifacts. A flow chart of patient enrollment is given in Fig. 1.

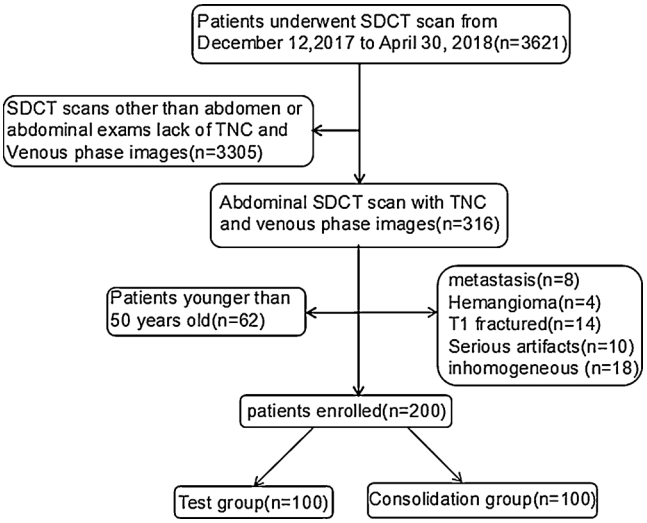

Fig. 1. Flowchart of study enrollment.

2.2. Image acquisition

All patients were imaged with a 64-detector row SDCT system (iQon Spectral CT, Philips Healthcare, Best, The Netherlands). TNC acquisitions were performed with the following parameters: tube voltage, 120 kV; tube current time product reference value, 66 mAs; dose right index, 12; liver area dose right index, +3. PVP post-contrast acquisitions were performed with the following parameters: tube voltage, 120 kV; tube current time product reference value, 116 mAs; dose right index, 17; liver area dose right index, +3. Conventional TNC and PVP post-contrast images were reconstructed with 3.0 mm section thickness and 1.5 mm interval using a standard soft tissue kernel and model-based iterative reconstruction (IMR level 1). For PVP post-contrast acquisitions, SBI were generated to allow for retrospective material decomposition. For contrast enhancement, a high-pressure injector was used to inject a contrast material volume of 95 ml (Accupaque 350 mgI/ml; GE Healthcare, Braunschweig, Germany) at a flow rate of 3.0 ml/s.

2.3. Image reconstruction and analysis

Reconstruction of VNC images and image analysis were performed using a dedicated CT image processing suite (IntelliSpace Portal, Version 9.0, Philips Healthcare). The upper part of L1 defined by the area between the cephalad endplate and the central vessel entry at the vertebral mid-portion was set on VNC images, TNC images, and PVP post-contrast images using double-oblique multiplanar reformations [16]. Oval regions of interest (ROI) as large as possible were placed in these reformatted sections through L1 without inclusion of cortical bone in each series. On the same section, a circular ROI as large as possible was placed in the abdominal aorta to assess VNC, TNC, and PVP CT attenuation values of the aorta (Fig. 2). Each measurement was taken three times, and the average CT attenuation value in HU was used for statistical analysis. Moreover, the anteroposterior and lateral diameters of the patients' abdomen were measured at the same level of L1 and were used to calculate the mean abdominal diameter. All ROIs were placed by one radiologist with 5 years of experience in osteoarticular system CT. Sex, age, and slice-specific tube current on a PVP post-contrast axial slice representing best the reformatted slice of L1 CT attenuation value assessment were recorded.

2.4. Statistical analysis

Student's *t* tests and Wilcoxon ranked tests were applied to compare CT attenuation values of L1 and the aorta on VNC, TNC, and PVP post-

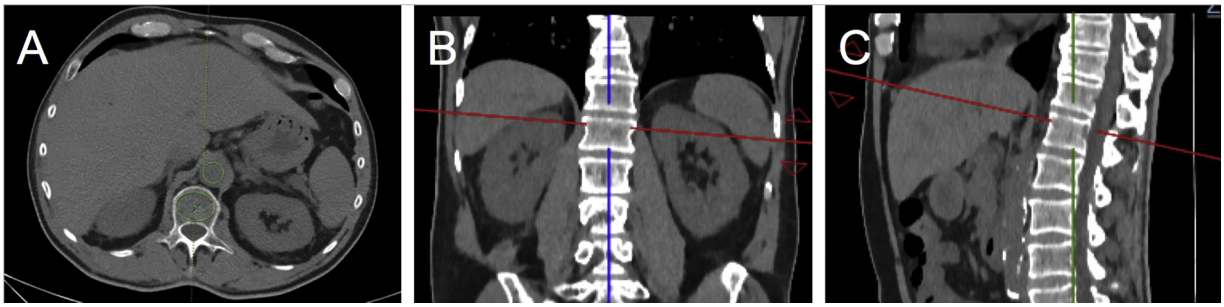

Fig. 2. Region of interest (ROI) placement in L1 and aorta on a virtual non-contrast image. An oval ROI is placed in the upper part of L1 between the endplate and the entrance of vessels at the midportion on an axial image (a). The coronal (b) and sagittal (c) reformation are used to angle the transverse plane in order to make it parallel with the endplate.

contrast images. The association between VNC and TNC L1 CT attenuation values was assessed using Pearson's correlation coefficient and multilinear regression analysis with backward elimination. The explanatory variables in the multilinear regression analysis were mean abdominal diameter, sex, age, tube current time product, and VNC L1 CT attenuation value. The regression equation established in the test group was applied to VNC L1 CT attenuation value in the validation group to predict TNC L1 CT attenuation value. A Bland-Altman plot was used to evaluate the agreement between the predicted TNC L1 CT attenuation value and the real TNC L1 CT attenuation value. Sensitivity, specificity, accuracy, and the area under the receiver operator characteristics curve (AUC) of VNC L1 CT attenuation value were calculated in the validation group for a CT attenuation value threshold of 110 HU for osteoporosis detection derived from the literature [7]. Statistical analyses were performed using SPSS (version 22.0; SPSS, Chicago, III) and MedCalc (version 15.8, Ostend, Belgium). $P < 0.05$ was considered to indicate statistical significance.

3. Results

3.1. Study patients

A flow chart of patient enrollment is given in Fig. 1. Clinical information of enrolled patients is summarized in Table 1. Of the 100 patients in the test group, there were 59 men with a mean age of 67.5 ± 9.7 years and 41 women with a mean age of 65.1 ± 8.2 years. Of the 100 patients in the validation group, there were 61 men with a mean age of 64.2 ± 10.0 years and 39 women with a mean age of 67.8 ± 11.4 years. Sex and age distribution as well as the mean abdominal diameter (30.6 ± 4.0 cm vs 30.8 ± 3.4 cm) did not differ between test group patients and validation group patients (P = 0.773, P = 0.241, and P = 0.687, respectively).

Table 1
Clinical information.

group	Test group (n)	Validation group (n)
Initial staging of cancer disease	13	21
Oncological follow-up	11	12
Work-up for suspected acute abdominal disease in out-patients	19	14
Work-up for suspected acute abdominal disease in in-patients	50	45
Work-up of liver cirrhosis	5	0
Suspected cancer disease	0	5
Other	2	3
total	100	100

3.2. Test group CT attenuation value

VNC L1 CT attenuation values were significantly lower than TNC L1 CT attenuation values (51.9 ± 25.7 HU vs 103.6 ± 41.3 HU, $P < 0.001$). The mean relative difference between VNC and TNC L1 CT attenuation values was -52.6 ± 13.0 %. TNC L1 CT attenuation values were significantly lower than PVP L1 CT attenuation values (103.6 ± 41.3 HU vs 125.6 ± 41.2 HU, $P < 0.001$). The mean attenuation increase from TNC to PVP was 22.0 ± 11.0 HU. There was no significant difference between VNC and TNC aortic CT attenuation values (37.6 ± 6.1 vs 37.1 ± 7.3 HU, $P = 0.354$). The mean attenuation increase from TNC to PVP was 98.0 ± 22.5 HU.

There was a linear positive correlation between VNC and TNC L1 CT attenuation values (r = 0.958, $P < 0.01$, Fig. 3) as well as between TNC and PVP L1 CT attenuation values (r = 0.964, $P < 0.001$). PVP L1 CT attenuation values were slightly negatively correlated with mean abdominal diameter (r = -0.346, $P < 0.001$).

In multilinear regression analysis, sex, age, mean abdominal diameter, and tube current were not significantly associated with L1 CT attenuation value decrease in VNC compared with TNC ($P = 0.802$, $P = 0.152$, $P = 0.918$, and $P = 0.429$, respectively). The final regression equation to predict the TNC L1 CT attenuation value from VNC images with the VNC L1 CT attenuation value as single independent variable was: pTNC = 23.677 + 1.540 x VNC, where pTNC is the predicted TNC L1 CT attenuation value and VNC is the VNC L1 CT attenuation value.

3.3. Validation group CT attenuation value

TNC L1 CT attenuation values (112.1 ± 38.3 HU), VNC L1 CT attenuation values (58.1 ± 24.4 HU), and PVP L1 CT attenuation values (134.1 ± 38.4 HU) of the validation group were not significantly

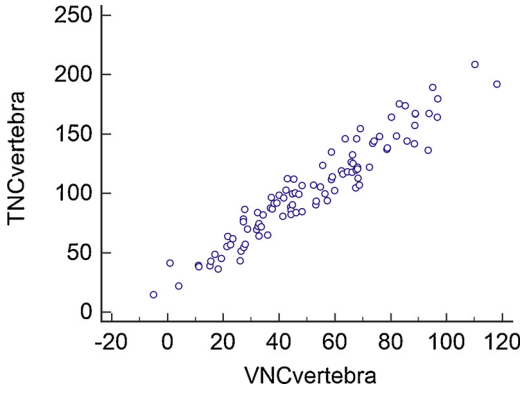

Fig. 3. Scatter plot of L1 CT attenuation value in test group. Graph shows a linear correlation between L1 CT attenuation values on VNC and TNC images in the test group. Coefficient of determination was r = 0.958 ($P < 0.01$).

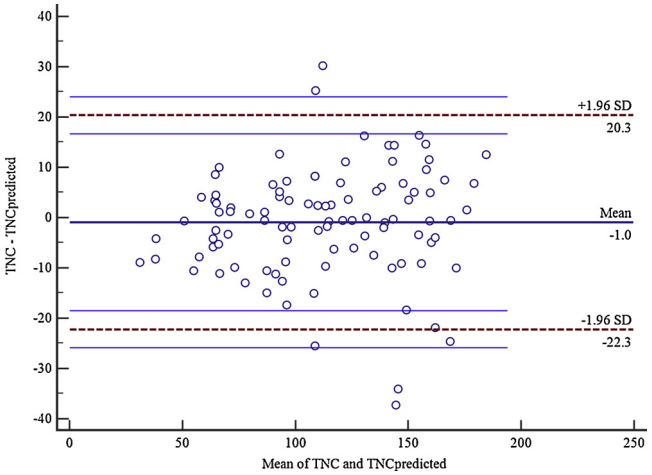

Fig. 4. Bland-Altman plot of true and predicted L1 CT attenuation values in the validation group.The graph shows that true TNC L1 CT attenuation values and TNC L1 CT attenuation values predicted from VNC L1 CT attenuation values ($TNC_{predicted}$) are in good agreement with the 95 % limits of agreements ranging from −22.3HU to 20.3HU.

different from the patients in the test group ($P = 0.133$, $P = 0.083$, and $P = 0.131$, respectively). Using the regression equation established in the test group, the predicted TNC L1 CT attenuation values (113.1 ± 37.5 HU) did not differ from the real TNC L1 CT attenuation values ($P = 0.359$). The Bland-Altman plot is presented in Fig. 4. Except for some outliers, the differences between predicted and real TNC L1 CT attenuation values were evenly spread around zero, and the 95 % limits of agreements ranged from −22.3HU to 20.3HU.

3.4. Performance of VNC L1 CT attenuation value to identify osteoporosis

In the validation group, a VNC L1 CT attenuation cut-off value of 52 HU for identification of osteoporosis compared with the reference standard cut-off value of 110 HU yielded a sensitivity, specificity, and accuracy of 89.1 %(41/46), 96.3 %(52/54), and 93.0 %(93/100), respectively. The AUC of a VNC L1 CT attenuation cut-off value of 52 HU was 0.978 (95 % confidence interval, 0.927-0.997) (Fig. 5).

4. Discussion

This study shows that the CT attenuation value of osseous structures is systematically underestimated when using VNC images compared with TNC images for bone density assessment using SDCT with reconstruction algorithms primarily designed for iodine removal from solid organs. However, there is a strong linear association between VNC and TNC CT attenuation values at the level of L1, and the TNC L1 CT attenuation value can be predicted using the formula derived in this study for SDCT. Despite of the CT attenuation value underestimation, VNC images may perform well in phantom-less opportunistic osteoporosis detection using CT attenuation value thresholds published by other groups.

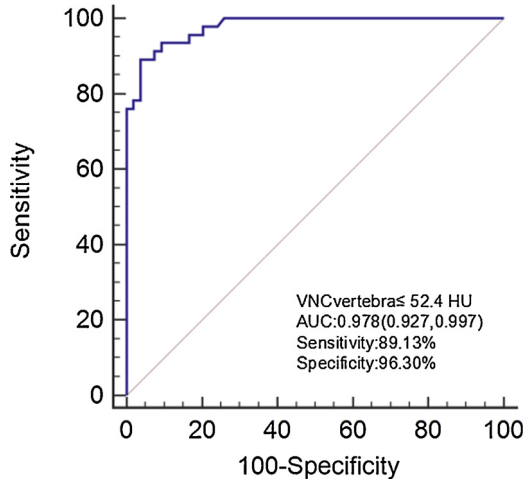

Fig. 5. ROC curve of VNC L1 CT attenuation value ($VNC_{vertebra}$) in validation group for osteoporosis detection.

Phantom-less opportunistic BMD measurements based on CT examinations performed for other indications were subject to several investigations in recent years, e.g. in the context of non-contrast CT colonography [8], non-contrast CT of the spine [17] and contrast-enhanced abdominal CT [7,18]. In these studies, CT attenuation values of the lumbar spine correlated well with values obtained from phantom-calibrated quantitative CT acquisitions or DXA BMD assessments.

Pickhardt et al. [7] proposed different thresholds of CT attenuation values for differentiation between osteoporosis and osteopenia or normal bone. In their study, a L1 CT attenuation value threshold of 110 HU was more than 90 % specific for distinguishing osteoporosis from non-osteoporosis and was suggested for patient groups considered to have a lower osteoporosis risk to minimize false-positive results. Other CT attenuation value thresholds were proposed for other patient populations and screening objectives. So, when determining the appropriate threshold for clinical use, the expected prevalence of osteoporosis in the patient population considered should be kept in mind. We found that a 52 HU threshold in SDCT VNC images corresponds to the 110 HU threshold proposed by Pickhardt et al. [7] and performs well for osteoporosis detection using this reference standard.

Ohara et al. [19] concluded that the average bone density of three thoracic vertebral bones was highly correlated with bone density in L1 alone. Pickhardt et al. [7] found that measurements at L1 were as or more accurate than the results at other levels, including multilevel assessment. Romme et al. [20] showed no added value of using three thoracic vertebral levels compared to one measurement at L1. Pompe et al. [16] reported on good to excellent inter-examination and inter-observer reliability of L1 CT attenuation value measurements. For these reasons, we only evaluated vertebral CT attenuation value on VNC, TNC, and post-contrast PVP images at the level of L1.

Our study confirms a significant increase of L1 CT attenuation values after intravenous contrast agent administration, which could result in underestimation of osteoporosis when not taken into account. Similar to our data, e.g. Pompe et al. [11] showed substantial differences between the attenuation values of L1 measured in different contrast phases with a mean difference around 20 HU between the pre-contrast phase and the post-contrast PVP. In the studies by Pompe et al. [11] and Acu et al. [21], the timing of the post-contrast phase did influence CT attenuation significantly. Effects of the volume of injected contrast material were not reported. We found a negative linear correlation between PVP L1 CT attenuation values and mean abdominal diameters using a contrast administration protocol that was not tailored individually according to body weight. This suggests that body size influences bone marrow enhancement and, thus, assessment of vertebral CT attenuation values on contrast enhanced images. The iodine concentration of the contrast agent may impact on the CT attenuation value of bone as well. Gerety et al. [22] have shown that the L1 CT attenuation value also depends on the acquisition parameters such as tube voltage. The tube voltage in our study using SDCT was always 120 kVp. According to our multivariate regression analysis, age, sex, and abdominal diameters, do not significantly influence the magnitude of L1 CT attenuation values in VNC images.

Ananthakrishnan et al. [15] presented the first study comparing attenuation values obtained from VNC images with those obtained from TNC images in the abdomen using SDCT. In their study, TNC and VNC CT attenuation values were equivalent e.g. for liver, spleen, and aorta. In our study, VNC density values of the abdominal aorta were similar to

TNC density values as well, suggesting again that material decomposition with virtual iodine removal works fine for non-osseous structures characterized by soft tissue equivalent CT attenuation. For calcium containing structures, however, the process of iodine subtraction to derive VNC images expectedly includes bone minerals of similar density leading to disproportionate decrease of the bone CT attenuation value in VNC images. Comparably, Moon et al. [23] suggested that subtracting iodine from post-contrast CT urographies may have negatively influenced the detection of small urinary stones in corresponding VNC images. In a cross-platform study by Sellerer et al., there were noticeable differences in material decomposition concerning iodine quantification between different dual-energy CT techniques with SDCT being slightly more accurate than dual-source CT [24]. Transferring this observation to iodine removal for reconstruction of VNC images, our data cannot be transferred to other scanner types without caution.

Recently, studies reported a high accuracy of phantom-less SDCT for quantitative BMD measurements in phantoms and vertebral specimens using known hydroxyapatite concentrations and conventional phantom-based quantitative CT or DXA, respectively, as reference standard [25,26]. Basically, in these studies, quantitative BMD values were derived from fitting the attenuation profiles of the sample established from different virtual monochromatic images to the attenuation profiles of hydroxyapatite. This approach represents a promising outlook to use spectral CT for BMD assessment but is still in a preclinical state.

Our study has limitations. First, the real prevalence of osteoporosis in our study groups is not known, as DXA or quantitative CT were not available. In fact, we have used a CT attenuation value threshold for defining presence of osteoporosis that was derived from the literature and is still under debate. Second, we did not perform an inter-observer and inter-examination reproducibility analysis. However, other groups have reported on low variability of ROI measurements of the L1 CT attenuation value [8,16,19]. Third, apart from the general increase of L1 CT attenuation value after contrast material administration and its negative correlation with mean abdominal diameters, we did not perform a sophisticated analysis of the effects of different contrast material injection parameters on L1 CT attenuation value.

5. Conclusions

In conclusion, we demonstrated that the TNC L1 CT attenuation value can be predicted by using the VNC L1 CT attenuation value using SDCT and that CT attenuation value thresholds for osteoporosis detection can be adapted to VNC images. Thus, VNC images are a feasible option for osteoporosis screening using SDCT acquisitions performed for other clinical indications under due consideration of the ongoing debate concerning phantom-less BMD assessment using CT.

Funding

This research did not receive any specific grant from funding agencies in the public, commercial, or not-for-profit sectors

Declaration of Competing Interest

None.

References

[1] L. Sànchez-Riera, E. Carnahan, T. Vos, L. Veerman, R. Norman, S.S. Lim, et al., The global burden attributable to low bone mineral density, Ann. Rheum. Dis. 73 (2014) 1635–1645, https://doi.org/10.1136/annrheumdis-2013-204320.

[2] B. Haussler, H. Gothe, D. Gol, G. Glaeske, L. Pientka, D. Felsenberg, Epidemiology, treatment and costs of osteoporosis in Germany–the BoneEVA Study, Osteoporos. Int. 18 (2007) 77–84, https://doi.org/10.1007/s00198-006-0206-y.

[3] J.R. Curtis, L. Carbone, H. Cheng, B. Hayes, A. Laster, R. Matthews, et al., Longitudinal trends in use of bone mass measurement among older americans, 1999-2005, J. Bone Miner. Res. 23 (2008) 1061–1067, https://doi.org/10.1359/jbmr.080232.

[4] J.A. Kanis, Assessment of fracture risk and its application to screening for postmenopausal osteoporosis: synopsis of a WHO report. WHO Study Group, Osteoporos Int. 4 (1994) 368–381.

[5] T.M. Link, Osteoporosis imaging: state of the art and advanced imaging, Radiology 263 (2012) 3–17, https://doi.org/10.1148/radiol.2633201203.

[6] C.F. Buckens, G. Dijkhuis, B. de Keizer, H.J. Verhaar, P.A. de Jong, Opportunistic screening for osteoporosis on routine computed tomography? An external validation study, Eur. Radiol. 25 (2015) 2074–2079, https://doi.org/10.1007/s00330-014-3584-0.

[7] P.J. Pickhardt, B.D. Pooler, T. Lauder, A.M. del Rio, R.J. Bruce, N. Binkley, Opportunistic screening for osteoporosis using abdominal computed tomography scans obtained for other indications, Ann. Intern. Med. 158 (2013) 588–595, https://doi.org/10.7326/0003-4819-158-8-201304160-00003.

[8] P.J. Pickhardt, L.J. Lee, A. Muñoz del Rio, T. Lauder, R.J. Bruce, R.M. Summers, et al., Simultaneous screening for osteoporosis at CT colonography: bone mineral density assessment using MDCT attenuation techniques compared with the DXA reference standard, J. Bone Miner. Res. 26 (2011) 2194–2203, https://doi.org/10.1002/jbmr.428.

[9] A.E. Papadakis, A.H. Karantanas, G. Papadokostakis, E. Petinellis, J. Damilakis, Can abdominal multi-detector CT diagnose spinal osteoporosis? Eur. Radiol. 19 (2009) 172–176, https://doi.org/10.1007/s00330-008-1099-2.

[10] H.W. Garner, M.M. Paturzo, G. Gaudier, P.J. Pickhardt, D.E. Wessell, Variation in attenuation in L1 trabecular bone at different tube voltages: caution is warranted when screening for osteoporosis with the use of opportunistic CT, Am. J. Roentgenol. 208 (2017) 165–170, https://doi.org/10.2214/AJR.16.16744.

[11] E. Pompe, M.J. Willemink, G.R. Dijkhuis, H.J.J. Verhaar, F.A.A. Mohamed Hoesein, P.A. de Jong, Intravenous contrast injection significantly affects bone mineral density measured on CT, Eur. Radiol. 25 (2015) 283–289, https://doi.org/10.1007/s00330-014-3408-2.

[12] A. Toelly, C. Bardach, M. Weber, R. Gong, Y. Lai, P. Wang, et al., Influence of contrast media on bone mineral density (BMD) measurements from routine contrast-enhanced MDCT datasets using a phantom-less BMD measurement tool, Rofo 189 (2017) 537–543, https://doi.org/10.1055/s-0043-102941.

[13] P.I. Mallinson, T.M. Coupal, P.D. McLaughlin, S. Nicolaou, P.L. Munk, H.A. Ouellette, Dual-energy CT for the musculoskeletal system, Radiology 281 (2016) 690–707, https://doi.org/10.1148/radiol.2016151109.

[14] C.H. McCollough, S. Leng, L. Yu, J.G. Fletcher, Dual- and multi-energy CT: principles, technical approaches, and clinical applications, Radiology 276 (2015) 637–653, https://doi.org/10.1148/radiol.2015142631.

[15] L. Ananthakrishnan, P. Rajiah, R. Ahn, N. Rassouli, Y. Xi, T.C. Soesbe, et al., Spectral detector CT-derived virtual non-contrast images: comparison of attenuation values with unenhanced CT, Abdom. Radiol. 42 (2017) 702–709, https://doi.org/10.1007/s00261-016-1036-9.

[16] E. Pompe, P.A. de Jong, W.U. de Jong, R.A.P. Takx, A.L.M. Eikendal, M.J. Willemink, et al., Inter-observer and inter-examination variability of manual vertebral bone attenuation measurements on computed tomography, Eur. Radiol. 26 (2016) 3046–3053, https://doi.org/10.1007/s00330-015-4145-x.

[17] B.J. Schwaiger, A.S. Gersing, T. Baum, P.B. Noel, C. Zimmer, J.S. Bauer, Bone mineral density values derived from routine lumbar spine multidetector row CT predict osteoporotic vertebral fractures and screw loosening, AJNR Am. J. Neuroradiol. 35 (2014) 1628–1633, https://doi.org/10.3174/ajnr.A3893.

[18] T. Baum, D. Müller, M. Dobritz, E.J. Rummeny, T.M. Link, J.S. Bauer, BMD measurements of the spine derived from sagittal reformations of contrast-enhanced MDCT without dedicated software, Eur. J. Radiol. 80 (2011) e140–5, , https://doi.org/10.1016/j.ejrad.2010.08.034.

[19] T. Ohara, T. Hirai, S. Muro, A. Haruna, K. Terada, D. Kinose, et al., Relationship between pulmonary emphysema and osteoporosis assessed by CT in patients with COPD, Chest 134 (2008) 1244–1249, https://doi.org/10.1378/chest.07-3054.

[20] E.A.P.M. Romme, J.T. Murchison, K.F. Phang, F.H. Jansen, E.P.A. Rutten, E.F.M. Wouters, et al., Bone attenuation on routine chest CT correlates with bone mineral density on DXA in patients with COPD, J. Bone Miner. Res. 27 (2012) 2338–2343, https://doi.org/10.1002/jbmr.1678.

[21] K. Acu, M. Scheel, A.S. Issever, Time dependency of bone density estimation from computed tomography with intravenous contrast agent administration, Osteoporos. Int. 25 (2014) 535–542, https://doi.org/10.1007/s00198-013-2440-4.

[22] E.-L. Gerety, P.W. Bearcroft, L1 vertebral density on CT is too variable with different scanning protocols to be a useful screening tool for osteoporosis in everyday practice, BJR 91 (2018) 20170395, https://doi.org/10.1259/bjr.20170395 20170395–28.

[23] J.W. Moon, B.K. Park, C.K. Kim, S.Y. Park, Evaluation of virtual unenhanced CT obtained from dual-energy CT urography for detecting urinary stones, BJR 85 (2012) e176–e181, https://doi.org/10.1259/bjr/19566194.

[24] T. Sellerer, P.B. Noël, M. Patino, A. Parakh, S. Ehn, S. Zeiter, et al., Dual-energy CT: a phantom comparison of different platforms for abdominal imaging, Eur. Radiol. 28 (2018) 1–11, https://doi.org/10.1007/s00330-017-5238-5.

[25] K. Mei, B.J. Schwaiger, F.K. Kopp, S. Ehn, A.S. Gersing, J.S. Kirschke, et al., Bone mineral density measurements in vertebral specimens and phantoms using dual-layer spectral computed tomography, Sci. Rep. 7 (2017) 1–10, https://doi.org/10.1038/s41598-017-17855-4.

[26] R.W. van Hamersvelt, A.M.R. Schilham, K. Engelke, A.M. den Harder, B. de Keizer, H.J. Verhaar, et al., Accuracy of bone mineral density quantification using dual-layer spectral detector CT: a phantom study, Eur. Radiol. 27 (2017) 4351–4359, https://doi.org/10.1007/s00330-017-4801-4.